European Journal of Mechanics / A Solids 91 (2022) 104412

Contents lists available at ScienceDirect

European Journal of Mechanics / A Solids

journal homepage: www.elsevier.com/locate/ejmsol

Investigation of the effect of cutout shape on thermal stresses in perforated multilayer composites subjected to heat flux using an analytical method

Mohammad Hossein Bayati Chaleshtari, Hadi Khoramishad *

School of Mechanical Engineering, Iran University of Science and Technology, Narmak, 16846, Tehran, Iran

ARTICLE INFO

Keywords:
Thermal stress
Non-circular cutout
Complex variable method
Symmetric composite laminate
Analytical solution

ABSTRACT

In the engineering design of perforated composite laminates, understanding the effect of geometrical and material parameters on stress concentration is of vital importance. In this paper, the effect of the cutout shape on the thermal stresses induced in perforated multilayer composite plates under uniform heat flux was studied. The thermal stress concentration was investigated using an analytical method based on the two-dimensional thermo-elastic theory, the Lekhnitskii method and conformal mapping by varying the laminate material and the aspect ratio, the bluntness and the rotation angle of the 3- to 6-sided polygonal cutouts. It was found out that the desirable cutout angular position for which the minimum thermal stress concentration was obtained was dependent on the order of the polygonal cutout, whereas the desirable cutout aspect ratio was unity irrespective of the cutout shape. The analytical results were in a reasonable correlation with the finite element results.

1. Introduction

The presence of cutouts with different geometries in structures is inevitable to meet service requirements in different industries. However, cutouts cause stress concentration in structures and can give rise to early failure if they are not considered properly. Hence, predicting stress concentration is crucial in achieving an acceptable structural design. Laminated composites are likely to be subjected to thermal loads. Therefore, estimating the induced thermal stress distribution in a laminated composite plate containing a cutout can be of high importance. The thermal stresses induced in a perforated laminated composite can be considerably influenced by the cutout geometry. The effect of the cutout shape on the thermal stress distribution in a perforated composite laminate can be predicted numerically and analytically. The analytical methods can be efficiently employed for parametric studies.

Many studies investigated the stress distribution in perforated single-layer isotropic and anisotropic plates subjected to mechanical or thermal loading. Muskhelishvili (1954) initially employed the complex variable method for solving the boundary value problems in two-dimensional elastic and isotropic materials. Savin (1961) utilized this technique to examine infinite isotropic plates with circular and elliptical cutouts. The method proposed by Muskhelisvili was extended to 2D problems concerning anisotropic elastic materials by Lekhnitskii (1969). He could successfully employ this method for obtaining an analytical solution for an infinite anisotropic plate containing a circular cutout of different sizes. Hasebe and Wang (2005) extended the formulation to tackle the 2D thermo-elastic problems concerning homogeneous and isotropic plates under different thermal and mechanical boundary conditions. Bhullar and Wegner (2009) used the complex variable method for analyzing an anisotropic plate with an elliptical cutout having isothermal conditions at its edges. Zeng et al. (2018) investigated stress distribution around two oval cutouts in an infinite plate using an analytical method. They employed conformal mapping function and complex variable method to obtain the stress distribution around cutouts when the plate was subjected to mechanical loading. Bayati Chaleshtari and Jafari (2017) used gray wolf optimization algorithm to achieve optimum stress in finite metallic plates containing a polygonal cutout. They applied an analytical method based on the complex variable method. Jafari and Bayati Chaleshtari (2017) determined the optimal values of the parameters affecting the normalized stress around a quasi-triangular cutout in an orthotropic plate. The design variables in this study were the loading angle, the cutout rotation angle and bluntness and the fiber angle. Cai et al. (2019) obtained the optimal shape of two cutouts with different areas in an infinite plate subjected to biaxial loads at infinity and internal uniform pressure on cutout boundaries using conformal mapping function and the complex variable method. Natsuki and Natsuki (2019) proposed an analytical model to investigate the residual thermal stress of graphene nanoribbons (GNRs) coated with

* Corresponding author.
E-mail address: Khoramishad@iust.ac.ir (H. Khoramishad).

https://doi.org/10.1016/j.euromechsol.2021.104412
Received 30 July 2019; Received in revised form 22 August 2021; Accepted 25 August 2021
Available online 1 September 2021

nano film. Jafari et al. (2016) achieved an analytical solution for a thermo-elastic problem comprising a plate with isotropic properties and a non-circular cutout under uniform heat flux. Sayman (2005) conducted thermal stress analysis for a symmetric aluminum based laminated plate. Mousanezhad Viyand et al. (2013) proposed an analytical method for determining the interlaminar stresses in symmetric composite laminates under mechanical loading using the Reddy's layer-wise theory. Rasouli and Jafari (2016) used the Lekhnitskii method and a conformal mapping technique to determine the stress distribution surrounding an elliptical cutout in an infinite anisotropic plate subjected to uniform heat flux. Nageswara Rao et al. (2010) used the Savin's formulation (Savin, 1961) for stress analysis in symmetric laminates containing a cutout with a general shape under arbitrary biaxial loading. They achieved the stress distribution surrounding the cutout using a mapping function. Sharma (2015) employed the complex variable method for obtaining the generalized solution for an infinite laminate with a polygonal cutout and considered two different layups of $[0/90]_s$ and $[45/-45]_s$. Ukadgaonker and Rao (2000) studied perforated laminates with symmetrical stacking sequences by employing a complex potential method and adapting the formulation given by Savin (1961) for stresses around cutouts in anisotropic plates under in-plane loading. Lal et al. (2012) conducted post-buckling analysis of FGMs plates under mechanical and thermal loadings with and without square and circular cutouts positioned at the plate center by using analytical solution. Jafari et al. (2018) used the Lekhnitskii method and a genetic algorithm to achieve optimum failure strength in symmetric composite laminates containing non-circular cutouts. Moure et al. (2017) investigated the matrix cracking evolution in an open-cutout composite laminate under single and combined thermal and mechanical loads. For this purpose, the discrete damage mechanics-based model of Barbero Cortes was amended to consider the effect of thermal loads. Jafari and Jafari (2019) investigated the stress distribution surrounding a rectangular cutout in an orthotropic infinite plate subjected to uniform heat flux.

The previous analytical studies conducted on the thermal stress analysis of perforated anisotropic plates have dealt with single-layer plates. In the present study, the thermal stress distribution in symmetric multilayer laminates with non-circular cutouts under uniform heat flux was investigated using an analytical method based on the complex variable method and a conformal mapping technique. The effect of the various shapes of cutout including triangular, square, pentagonal and hexagonal was analytically studied on the thermal stress distribution surrounding the cutout. In addition to that, the effects of the laminate material, the bluntness, the rotation angle and the aspect ratio of cutout were studied.

2. Problem definition

Uniform heat flux within a perforated plate is disturbed due to the presence of a thermally insulated non-circular cutout. As shown in Fig. 1, the laminate was under the remote uniform heat flux q in a steady-state condition.

Due to the absence of a heat source in the laminate, the maximum stress occurred on the cutout edges. According to a coordinate system with normal and tangential coordinates (ρ,θ) (see Fig. 1), only the tangential stress component (σ_θ) was non-zero at the cutout edges.

The assumptions considered in this study for solving the problem were as follows:

- The symmetric laminate was assumed to be linear elastic and anisotropic governed by the generalized Hooke's law.
- The edges of the non-circular cutouts were thermally insulated.
- The cutout size was small enough in comparison with the dimensions of the laminate so the laminate was considered infinite.
- The Neumann boundary condition was considered for the cutout.
- The heat flux angle (δ) was considered 270°.

3. Analytical solution

The relationship between the mid-plane stress and strain, the mid-plane curvature and thermal strain can be obtained as Eq. (1) using the theory of classical laminated plate theory (CLPT) (Herakovich, 1998).

$$\{\sigma_{xy}\}^l = \left[\overline{Q}_{ij}\right]^l \left[\left\{\varepsilon^0_{xy}\right\} + z\{\chi_{xy}\} - \{\varepsilon_{xy}\}^T\right] \tag{1}$$

where $[\overline{Q}_{ij}]$ is the reduced stiffness matrix for the lth layer, $\{\varepsilon^0_{xy}\}$ and $\{\chi_{xy}\}$ are the mid-plane strain and curvature vectors and the superscript T stands for thermal. Two coordinate systems including the global (off-axis; x, y, z) and the local (on-axis; x_1, x_2, x_3) coordinate systems were considered. The local coordinate system was specified based on the fiber direction in each layer, in which x_1, x_2 and x_3 are the coordinates parallel, in-plane perpendicular and out-of-plane perpendicular to the fiber direction, respectively. The total strain can be obtained by the summation of the mid-plane strain and the strain related to curvature. The mid-plane strain and curvature vectors can be defined as Eq. (2).

$$\begin{Bmatrix} \varepsilon^0_x \\ \varepsilon^0_y \\ \gamma^0_{xy} \end{Bmatrix} = \begin{Bmatrix} \dfrac{\partial u_0}{\partial x} \\ \dfrac{\partial v_0}{\partial y} \\ \dfrac{\partial u_0}{\partial y} + \dfrac{\partial v_0}{\partial x} \end{Bmatrix}, \begin{Bmatrix} \chi_x \\ \chi_y \\ \chi_{xy} \end{Bmatrix} = -\begin{Bmatrix} \dfrac{\partial^2 w_0}{\partial x^2} \\ \dfrac{\partial^2 w_0}{\partial y^2} \\ 2\dfrac{\partial^2 w_0}{\partial x \partial y} \end{Bmatrix}, \tag{2}$$

in which u_0, v_0 and w_0 are the x, y and z mid-plane displacement components, respectively. The stress resultants ($[N]$) and the moments ($[M]$) can be obtained by integrating stress in each layer over the multilayer

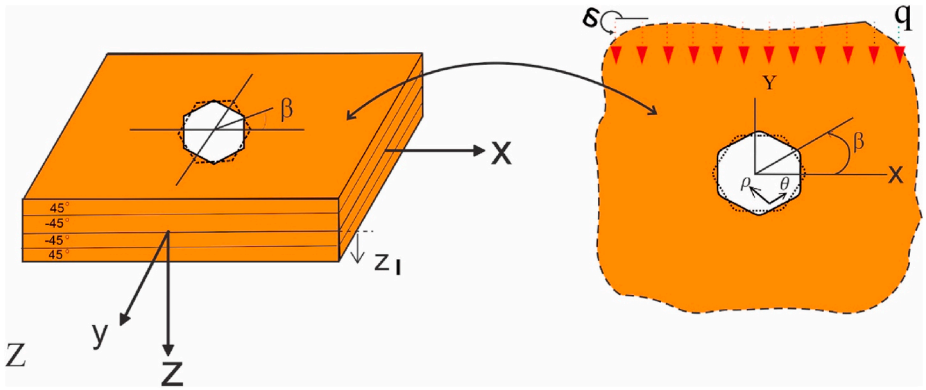

Fig. 1. A symmetric composite laminate containing quasi-hexagonal cutout.

thickness by Eq. (3) (Joshi et al., 2017).

$$[N] = \int_{-H/2}^{H/2} \{\sigma_{xy}\}dz = \sum_{l=1}^{N_L} \int_{z_{l-1}}^{z_l} \{\sigma_{xy}\}^l dz$$
$$[M] = \int_{-H/2}^{H/2} \{\sigma_{xy}\}zdz = \sum_{l=1}^{N_L} \int_{z_{l-1}}^{z_l} \{\sigma_{xy}\}^l zdz \quad (3)$$

where N_L is the number of total layers. By replacing (1) into (3), the stress resultants and moments can be presented as Eq. (4).

$$[N] = \sum_{l=1}^{N_L} \int_{z_{l-1}}^{z_l} \left[\overline{Q}\right]^l \{\varepsilon_{xy}{}^0\}dz + \sum_{l=1}^{N_L} \int_{z_{l-1}}^{z_l} \left[\overline{Q}\right]^l \{\chi_{xy}\}zdz - \sum_{l=1}^{N_L} \int_{z_{l-1}}^{z_l} \left[\overline{Q}\right]^l \{\varepsilon_{xy}{}^T\}^l dz$$
$$[M] = \sum_{l=1}^{N_L} \int_{z_{l-1}}^{z_l} \left[\overline{Q}\right]^l \{\varepsilon_{xy}{}^0\}zdz + \sum_{l=1}^{N_L} \int_{z_{l-1}}^{z_l} \left[\overline{Q}\right]^l \{\chi_{xy}\}z^2dz - \sum_{l=1}^{N_L} \int_{z_{l-1}}^{z_l} \left[\overline{Q}\right]^l \{\varepsilon_{xy}{}^T\}^l zdz \quad (4)$$

In Eq. (4), z_l and z_{l-1} represent the z components of the upper and lower boundaries of the lth layer as shown in Fig. 2.

Eq. (4) can be rewritten as Eq. (5).

$$\begin{Bmatrix} N_x \\ N_y \\ N_{xy} \\ M_x \\ M_y \\ M_{xy} \end{Bmatrix} = \begin{bmatrix} A_{11} & A_{12} & A_{16} & B_{11} & B_{12} & B_{16} \\ A_{12} & A_{22} & A_{26} & B_{12} & B_{22} & B_{26} \\ A_{16} & A_{26} & A_{66} & B_{16} & B_{26} & B_{66} \\ B_{11} & B_{12} & B_{16} & D_{11} & D_{12} & D_{16} \\ B_{12} & B_{22} & B_{26} & D_{12} & D_{22} & D_{26} \\ B_{16} & B_{26} & B_{66} & D_{66} & D_{26} & D_{66} \end{bmatrix} \begin{Bmatrix} \varepsilon_x^0 \\ \varepsilon_y^0 \\ \varepsilon_{xy}^0 \\ \chi_x \\ \chi_y \\ \chi_{xy} \end{Bmatrix} - \begin{Bmatrix} N_x \\ N_y \\ N_{xy} \\ M_x \\ M_y \\ M_{xy} \end{Bmatrix}^T \quad (5)$$

In Eq. (5), due to the absence of external torque and the symmetry of laminate, the matrices $[D_{ij}]$ and $[B_{ij}]$ are zero and the matrix $[A_{ij}]$ is defined in Eq. (6).

$$A_{ij} = \sum_{l=1}^{N_L} \left[\overline{Q}\right]^l (z_l - z_{l-1}) \quad (6)$$

Therefore, the resultants of thermal stress can be obtained in the form of Eq. (7).

$$\{N\}^T = \sum_{l=1}^{N_L} \int_{z_{l-1}}^{z_l} \left[\overline{Q}_{ij}\right]^l \left(\{\varepsilon_{xy}\}^T\right)^l dz \quad (7)$$

The relation between the off-axis stress and strain components can be expressed as Eq. (8).

$$\{\varepsilon_{xy}\} = H[A]^{-1}\left[\{\sigma_{xy}\} + \{\sigma_{xy}{}^T\}\right] \quad (8)$$

in which H is the total thickness of the laminate. The thermal stress vector can be presented as Eq. (9).

$$\begin{Bmatrix} \sigma_x \\ \sigma_y \\ \tau_{xy} \end{Bmatrix}^T = \frac{1}{H} \sum_{l=1}^{N_L} \begin{bmatrix} \overline{Q}_{11} & \overline{Q}_{12} & \overline{Q}_{16} \\ \overline{Q}_{12} & \overline{Q}_{22} & \overline{Q}_{26} \\ \overline{Q}_{16} & \overline{Q}_{26} & \overline{Q}_{66} \end{bmatrix}^l \begin{Bmatrix} \overline{\alpha_x}\,\overline{\alpha_y} & \overline{\alpha_{xy}} \end{Bmatrix}^l (z_l - z_{l-1}).T \quad (9)$$

where T is the change in temperature and $\{\overline{\alpha}\}^l$ is the vector of the off-axis coefficients of thermal expansion of the lth layer with the components presented in Eq. (10).

$$\overline{\alpha_x} = \alpha_{11}m^2 + \alpha_{22}n^2,\ \overline{\alpha_y} = \alpha_{11}n^2 + \alpha_{22}m^2,\ \overline{\alpha_{xy}} = 2mn(\alpha_{11} - \alpha_{22}) \quad (10)$$

where α_{11} and α_{22} are the on-axis coefficients of thermal expansion. Moreover, m and n are the cosine and sine of the fiber angle γ, respectively. Eq. (9) can be rewritten as $\{\sigma\}^T = \{\Omega\}.T$ in which $\{\Omega\}$ is defined as Eq. (11).

$$\begin{Bmatrix} \Omega_x \\ \Omega_y \\ \Omega_{xy} \end{Bmatrix} = \frac{1}{H} \sum_{l=1}^{N} \begin{bmatrix} \overline{Q}_{11} & \overline{Q}_{12} & \overline{Q}_{16} \\ \overline{Q}_{12} & \overline{Q}_{22} & \overline{Q}_{26} \\ \overline{Q}_{16} & \overline{Q}_{26} & \overline{Q}_{66} \end{bmatrix}^l \begin{Bmatrix} \overline{\alpha_x}\,\overline{\alpha_y} & \overline{\alpha_{xy}} \end{Bmatrix}^l (z_l - z_{l-1}) \quad (11)$$

According to the Likhnitskii complex method and by considering the airy's stress function $U(x, y)$, the stress components are defined as Eq. (12).

$$\sigma_x = \frac{\partial^2 U}{\partial y^2},\ \sigma_y = \frac{\partial^2 U}{\partial x^2}, \tau_{xy} = -\frac{\partial^2 U}{\partial x \partial y}, \quad (12)$$

In two-dimensional problems, the compatibility equation can be expressed as Eq. (13).

$$\frac{\partial^2 \varepsilon_x}{\partial y^2} + \frac{\partial^2 \varepsilon_y}{\partial x^2} = \frac{\partial^2 \gamma_{xy}}{\partial x \partial y} \quad (13)$$

By substituting Eq. (12) into Eq. (8) and considering the compatibility equation (Eq. (13)) and rearranging the resultant equation, the constitutive equation for an anisotropic material can be obtained in terms of the stress function as Eq. (14).

$$a_{11}\frac{\partial^4 U}{\partial y^4} - 2a_{16}\frac{\partial^4 U}{\partial x \partial y^3} + (2a_{12} + a_{66})\frac{\partial^4 U}{\partial x^2 \partial y^2} - 2a_{26}\frac{\partial^4 U}{\partial x^3 \partial y} + a_{22}\frac{\partial^4 U}{\partial x^4} = -\alpha_x\frac{\partial^2 T}{\partial y^2} + \alpha_{xy}\frac{\partial^2 T}{\partial x \partial y} - \alpha_y\frac{\partial^2 T}{\partial x^2} \quad (14)$$

where a_{ij} are the components of the reduced compliance matrix ($[a] = [A]^{-1}$) and $\alpha_x, \alpha_y, \alpha_{xy}$ are the thermal expansion coefficients in the global coordinate system that can be obtained as Eq. (15). It should be noted that the overall laminate thickness was assumed unity.

$$\begin{aligned} \alpha_x &= a_{11}\Omega_x + a_{12}\Omega_y + a_{16}\Omega_{xy} \\ \alpha_y &= a_{12}\Omega_x + a_{22}\Omega_y + a_{26}\Omega_{xy} \\ \alpha_{xy} &= a_{16}\Omega_x + a_{26}\Omega_y + a_{66}\Omega_{xy} \end{aligned} \quad (15)$$

The general solution of Eq. (14) is as Eq. (16).

$$U = U^{(h)} + U^{(p)} \quad (16)$$

in which $U^{(h)}$ and $U^{(p)}$ are the homogeneous and particular parts of the solution of Eq. (14), respectively. The homogeneous part of the solution can be determined by solving Eq. (17).

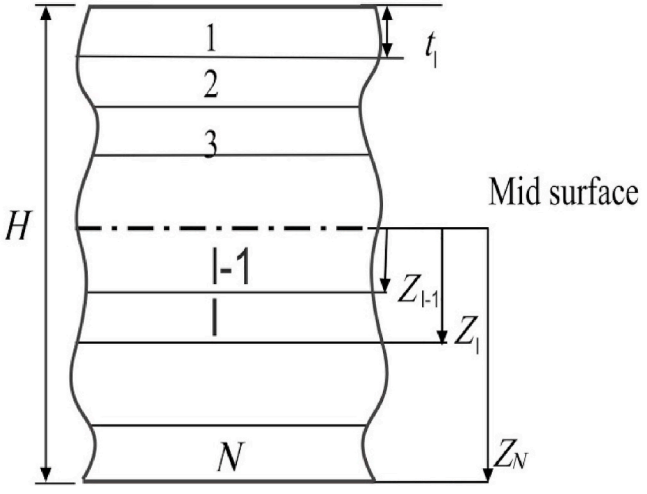

Fig. 2. The geometry of an N-layered laminate.

$$a_{11}\frac{\partial^4 U^{(h)}}{\partial y^4}-2a_{16}\frac{\partial^4 U^{(h)}}{\partial x\partial y^3}+(2a_{12}+a_{66})\frac{\partial^4 U^{(h)}}{\partial x^2\partial y^2}-2a_{26}\frac{\partial^4 U^{(h)}}{\partial x^3\partial y}+a_{22}\frac{\partial^4 U^{(h)}}{\partial x^4}=0 \tag{17}$$

Using four first-order linear differential operators (D_k), Eq. (17) can be expressed as Eq. (18) (Lekhnitskii, 1969).

$$D_1D_2D_3D_4U^{(h)}=0\ ,\ D_k=\frac{\partial}{\partial y}-\mu_k\frac{\partial}{\partial x},\ (k=1,2,3,4) \tag{18}$$

in which $\mu_k(k = 1,2,3,4)$ are the roots of the characteristic Eq. (19).

$$a_{11}\mu^4-2a_{16}\mu^3+(2a_{12}+a_{66})\mu^2-2a_{26}\mu+a_{22}=0 \tag{19}$$

The roots of Eq. (19) can be considered as Eq. (20).

$$\mu_1=\alpha_1+i\beta_1,\quad \mu_2=\overline{\mu_1}=\alpha_1-i\beta_1\quad \mu_3=\alpha_2+i\beta_2,\quad \mu_4=\overline{\mu_3}=\alpha_2-i\beta_2 \tag{20}$$

where α_1, α_2 ,β_1 and β_2 are real numbers. For a symmetric laminate $a_{16} = a_{26} = 0$, so the characteristic equation can be presented as Eq. (21).

$$a_{11}\mu^4+(2a_{12}+a_{66})\mu^2+a_{22}=0 \tag{21}$$

The function $U^{(h)}$ is considered as Eq. (22).

$$U^{(h)}=2\mathrm{Re}\sum_{k=1}^{2}U_k(Z_k) \tag{22}$$

where Z_k is the mapping function and is defined as Eq. (23).

$$Z_k=x+\mu_k y\quad k=1,2 \tag{23}$$

By substituting Eq. (22) into Eq. (17), the function $U^{(h)}$ can be obtained and consequently Eq. (16) is rewritten in the form of Eq. (24).

$$U=U_1(Z_1)+U_2(Z_2)+\overline{U_1(Z_1)}+\overline{U_2(Z_2)}+U^{(p)} \tag{24}$$

Now, the new stress function (ψ) is derived from the stress function U in the form of Eq. (25).

$$\frac{dU}{dz}=\psi_1(Z_1)+\psi_2(Z_2)+\overline{\psi_1(Z_1)}+\overline{\psi_2(Z_2)}+\psi^{(p)} \tag{25}$$

By substituting Eqs. (25) and (24) into Eq. (12), the stress components are determined as Eq. (26).

$$\begin{aligned}\sigma_x&=2\mathrm{Re}\{\mu_1^{\,2}\psi_1'(Z_1)+\mu_2^{\,2}\psi_2'(Z_2)\}+\frac{\partial^2U^{(p)}}{\partial y^2}\\ \sigma_y&=2\mathrm{Re}\{\psi_1'(Z_1)+\psi_2'(Z_2)\}+\frac{\partial^2U^{(p)}}{\partial x^2}\\ \tau_{xy}&=-2\mathrm{Re}\{\mu_1\psi_1'(Z_1)+\mu_2\psi_2'(Z_2)\}-\frac{\partial^2U^{(p)}}{\partial x\partial y}\end{aligned} \tag{26}$$

in which $\psi_1'(Z_1)$ and $\psi_2'(Z_2)$ are the derivatives of the functions $\psi_1(Z_1)$ and $\psi_2(Z_2)$ with respect to Z_1 and Z_2, respectively. To relate the on-axis heat flux q and temperature gradient in an orthotropic laminate, the Fourier's law was employed in the form of Eq. (27) (Ozisik, 1993).

$$\{q\}_{on}=-[k]_{on}\{\nabla T\}_{on} \tag{27}$$

In Eq. (27), $[k]_{on}$ is the on-axis anisotropic thermal conductivity matrix and T is the temperature change. It was assumed that the unidirectional laminae are isotropic in a plane normal to the fibers (i.e. transversely isotropic). Using the transformation matrix, Eq. (27) can be rewritten based on the off-axis coordinates as follows:

$$[T(\gamma)]\{q\}_{off}=-[k]_{on}[T(\gamma)]\{\nabla T\}_{off} \tag{28}$$

where $T(\gamma)$ is the inverse of the transformation matrix ($T(-\gamma)$) and is defined as Eq. (29).

$$T(\gamma)=\begin{bmatrix}\cos\gamma & \sin\gamma & 0\\ -\sin\gamma & \cos\gamma & 0\\ 0 & 0 & 1\end{bmatrix} \tag{29}$$

Therefore, the Fourier's law of thermal conduction in the global coordinate system can be presented as Eq. (30).

$$\{q\}_{off}=-[k]_{off}\{\nabla T\}_{off} \tag{30}$$

As a result, the off-axis thermal conductivity matrix can be obtained using Eq. (31) in terms of the on-axis thermal conductivities and fiber direction in a lamina.

$$[k]_{off}=[T(-\gamma)][k]_{on}[T(\gamma)] \tag{31}$$

By considering $n=\sin\gamma$ and $m=\cos\gamma$, the components of the off-axis thermal conductivity matrix $[k]_{off}=[\bar{k}]$ are defined as Eq. (32).

$$\begin{aligned}&\bar{k}_{11}=m^2k_{11}+n^2k_{22}\ \ \bar{k}_{12}=mn(k_{22}-k_{11})\\ &\bar{k}_{22}=n^2k_{11}+m^2k_{22}\ \bar{k}_{13}=\bar{k}_{23}=0\\ &\bar{k}_{33}=k_{22}\end{aligned} \tag{32}$$

By integrating the off-axis thermal conductivity coefficients across the laminate thickness, the resultant of thermal conductivity coefficients for a multilayer laminate can be determined using Eq. (33).

$$[K]=\int_{-H/2}^{H/2}\left[\bar{k}\right]^l dz=\sum_{l=1}^{N_L}\int_{z_{l-1}}^{z_l}\left[\bar{k}\right]^l dz \tag{33}$$

in which, $[K]$ is the thermal conductivity resultant matrix. Moreover, for a laminate without an internal heat source or sink we have:

$$\nabla.q_i=0 \tag{34}$$

By combining Eqs. (27) and (34), the governing thermal equation can be expressed as Eq. (35).

$$K_x\frac{\partial^2T}{\partial x^2}+2K_{xy}\frac{\partial^2T}{\partial x\partial y}+K_y\frac{\partial^2T}{\partial y^2}=0 \tag{35}$$

The temperature function ($T(x,y)$) is a harmonic function satisfying Eq. (35). The solution of Eq. (35) can be considered as $T = U(x + \mu_t y)$ in which μ_t are the roots of the characteristic Eq. (36).

$$K_y\mu_t^{\,2}+2K_{xy}\mu_t+K_x=0 \tag{36}$$

The thermal conductivity matrix is invertible and positive definite ($K_xK_y > K_{xy}^{\,2}$). Therefore, the characteristic Eq. (36) has a pair of complex conjugate roots and the solution of Eq. (35) can be written as Eq. (37) in which U_t is a complex function (Tarn and Wang, 1993).

$$\begin{aligned}&T=U_t(Z_t)+\overline{U_t(Z_t)}=2\mathrm{Re}(U_t(Z_t))\\ &Z_t=x+\mu_t y\end{aligned} \tag{37}$$

The particular solution of the stress function U (Eq. (38)) can be obtained by the substitution of Eq. (37) into Eq. (14).

$$U^{(p)}=2\mathrm{Re}(\eta U_t(Z_t)) \tag{38}$$

in which η is defined as follows:

$$\eta = \frac{\left(-\alpha_y + \alpha_{xy}\mu_t - \alpha_x{\mu_t}^2\right)}{a_{11}{\mu_t}^4 - 2a_{16}{\mu_t}^3 + (2a_{12}+a_{66}){\mu_t}^2 - 2a_{26}\mu_t + a_{22}} \tag{39}$$

Moreover, by substituting Eq. (38) into Eq. (26), the stress components are achieved using Eq. (40) as the functions of the stress functions.

$$\sigma_x = 2\mathrm{Re}\left\{{\mu_1}^2{\psi_1}'(Z_1) + {\mu_2}^2{\psi_2}'(Z_2)\right\} + 2\mathrm{Re}\left(\eta{\mu_t}^2{\psi_t}'\right)\ \sigma_y = 2\mathrm{Re}\left\{{\psi_1}'(Z_1) + {\psi_2}'(Z_2)\right\} + 2\mathrm{Re}(\eta{\psi_t}')\ \tau_{xy} = -2\mathrm{Re}\left\{\mu_1{\psi_1}'(Z_1) + \mu_2{\psi_2}'(Z_2)\right\} - 2\mathrm{Re}(\eta\mu_t{\psi_t}') \tag{40}$$

Based on Eq. (40), to achieve the stress components, the stress functions ψ_1, ψ_2 and ψ_t are required. To simply the formulations, four matrices are defined as Eq. (41) (Tarn and Wang, 1993).

$$L = \begin{bmatrix} -\mu_1 & -\mu_2 \\ 1 & 1 \end{bmatrix},\ l = \begin{bmatrix} -\eta\mu_t \\ \eta \end{bmatrix},\ \psi = \begin{bmatrix} \psi_1 \\ \psi_2 \end{bmatrix},\ A^{\wp} = \begin{bmatrix} p_1 & p_2 \\ q_1 & q_2 \end{bmatrix} \tag{41}$$

As, the boundary of the non-circular cutout was free from the external load, therefore the mechanical boundary condition of cutout can be considered as Eq. (42).

$$L\psi + \overline{L\psi} + l\psi_t + \overline{l\psi_t} = 0 \tag{42}$$

Moreover, as the boundary of the non-circular cutout was insulated, the Newman boundary condition can be used as Eq. (43).

$${\psi_t}'(\xi) - \overline{{\psi_t}'(\xi)} = 0 \tag{43}$$

The function ${\psi_t}'(\xi)$ can be defined by Eq. (44) using two functions $f_t(\xi)$ and $g_t(\xi)$ that are holomorphic in the inner and outer regions of the unit circle, respectively (Tarn and Wang, 1993).

$${\psi_t}'(\xi) = f_t(\xi) + g_t(\xi) \tag{44}$$

By considering the points on the cutout boundary ($\xi = \sigma$) and substituting Eq. (44) into Eq. (43) and multiplying it by the expression $\frac{d\sigma}{2\pi i(\sigma-\xi)}$ and utilizing the Cauchy integral, ${\psi_t}'(\xi)$ can be obtained as Eq. (45).

$${\psi_t}'(\xi) = f_t(\xi) + \overline{f}_t\left(\xi^{-1}\right) \tag{45}$$

The function ${\psi_t}'(\xi)$ can be presented as the Laurent series in which the term ξ^{-1} exists, hence by integrating ${\psi_t}'(\xi)$ with respect to ξ, the function $\psi_t(\xi)$ contains the term $\log\xi$ and can be expressed as Eq. (46).

$$\psi_t(\xi) = F_t(\xi) + G_t(\xi) + \Gamma\log\xi \tag{46}$$

in which $F_t(\xi)$ and $G_t(\xi)$ are holomorphic functions inside and outside the unit circle, respectively. Furthermore, the function $\psi(\xi)$ can be considered as Eq. (47) (Chao and Shen, 1998).

$$\psi(\xi) = f(\xi) + g(\xi) + h\log\xi \tag{47}$$

where $f(\xi)$ and $g(\xi)$ are the holomorphic functions inside and outside the unit circle, respectively. By substituting Eqs. (46) and (47) into Eq. (42) and multiplying it in $\frac{d\sigma}{2\pi i(\sigma-\xi)}$ and applying the Cauchy integral, $\psi(\xi)$ can be rephrased as Eq. (48).

$$\psi(\xi) = f(\xi) - L^{-1}\overline{Lf}\left(\xi^{-1}\right) - L^{-1}lG_t(\xi) - L^{-1}\overline{lF}_t\left(\xi^{-1}\right) + h\log\xi \tag{48}$$

where

$$h = L^{-1}\left(\overline{B} - B\right)^{-1}\left(\Gamma a - \overline{\Gamma a}\right) + A^{\wp-1}\left(\overline{B}^{-1} - B^{-1}\right)^{-1}\left(\Gamma l - \overline{\Gamma l}\right) \tag{49}$$

$$B = A^{\wp}L^{-1}$$

L and $A^{\wp}$ are defined in Eq. (41) and Γ can be obtained using the boundary conditions. When heat flux was applied to an anisotropic laminate with no cutout, the thermal stress function can be presented as Eq. (50) (Tarn and Wang, 1993).

$${\psi_t^{\infty}}' = \kappa Z_t \tag{50}$$

in which

$$\kappa = \frac{q(\cos\delta + \overline{\mu_t}\sin\delta)}{K_t(\mu_t - \overline{\mu_t})}$$
$$K_t = i\left(K_xK_y - {K_{xy}}^2\right)^{\frac{1}{2}} \tag{51}$$

in which δ is the heat flux angle. However, in the presence of a non-circular cutout, in addition to ${\psi_t^{\infty}}'$, the function ${\psi_t^{M}}'$ which is a holomorphic function outside the unit circle, should be incorporated into the thermal stress function. Therefore, the stress function can be expressed as Eq. (52).

$${\psi_t}'(\xi) = \kappa\left(\Delta_{1t}\xi + \Delta_{2t}\xi^{-1} + \Delta_{3t}\xi^{n} + \Delta_{4t}\xi^{-n}\right) + {\psi_t^{M}}'(\xi) \tag{52}$$

By comparing Eq. (52) and Eq. (45), the function $f_t(\xi)$ is defined as Eq. (53).

$$f_t(\xi) = \kappa\Delta_{1t}\xi + \kappa\Delta_{3t}\xi^{n} \tag{53}$$

Therefore, ${\psi_t}'(\xi)$ is determined as Eq. (54).

$${\psi_t}'(\xi) = \kappa\Delta_{1t}\xi + \overline{\kappa\Delta_{1t}}\xi^{-1} + \kappa\Delta_{3t}\xi^{n} + \overline{\kappa\Delta_{3t}}\xi^{-n} \tag{54}$$

By integrating Eq. (54) and comparing the result with Eq. (46), Γ can be obtained as Eq. (55).

$$\Gamma = -\Delta_{1t}(\kappa\Delta_{2t} - \overline{\kappa\Delta_{1t}}) - n\Delta_{3t}(\kappa\Delta_{4t} - \overline{\kappa\Delta_{3t}}) \tag{55}$$

As pointed out, ${\psi_t^{\infty}}'$ presents the thermal stress function for a laminate without any cutout. Hence, it can just cause the laminate deformation without stress. Hence, for achieving the thermal stress components in the presence of cutout, it is enough to determine ${\psi_t^{M}}'$ using Eqs. (50), (52) and (53) as follows:

$${\psi_t^{M}}'(\xi) = -(\kappa\Delta_{2t} - \overline{\kappa\Delta_{1t}})\xi^{-1} - (\kappa\Delta_{4t} - \overline{\kappa\Delta_{3t}})\xi^{-n} \tag{56}$$

By integrating Eq. (56), ψ_t^{M} can be obtained as Eq. (57).

$$\begin{aligned}\psi_t^{M}(\xi) = {} & [-\Delta_{1t}(\kappa\Delta_{2t} - \overline{\kappa\Delta_{1t}}) - n\Delta_{3t}(\kappa\Delta_{4t} - \overline{\kappa\Delta_{3t}})]\log\xi \\ & + \frac{1}{n-1}[\Delta_{1t}(\kappa\Delta_{4t} - \overline{\kappa\Delta_{3t}})]\xi^{-n+1} - \frac{1}{2}[\Delta_{2t}(\kappa\Delta_{2t} - \overline{\kappa\Delta_{1t}})]\xi^{-2} \\ & - \frac{1}{n+1}[\Delta_{2t}(\kappa\Delta_{4t} - \overline{\kappa\Delta_{3t}}) + n\Delta_{4t}(\kappa\Delta_{2t} - \overline{\kappa\Delta_{1t}})]\xi^{-n-1} \\ & - \frac{1}{n-1}[n\Delta_{3t}(\kappa\Delta_{2t} - \overline{\kappa\Delta_{1t}})]\xi^{n-2} - \frac{1}{2n}[n\Delta_{4t}(\kappa\Delta_{4t} - \overline{\kappa\Delta_{3t}})]\xi^{2n}\end{aligned} \tag{57}$$

By comparing Eqs. (57) and (46), the functions $F_t(\xi)$ and $G_t(\xi)$ are obtained and by inserting them into Eq. (48), the function $\psi(\xi)$ is achieved. Finally, the stress components can be obtained using Eq. (40).

3.1. The conformal mapping

The analytical solution of a circular cutout was extended to a non-circular cutout by mapping the infinite region outside the non-circular cutout to the outside region of a unit circle according to Fig. 3.

The mapping function used in this study is defined as Eq. (58).

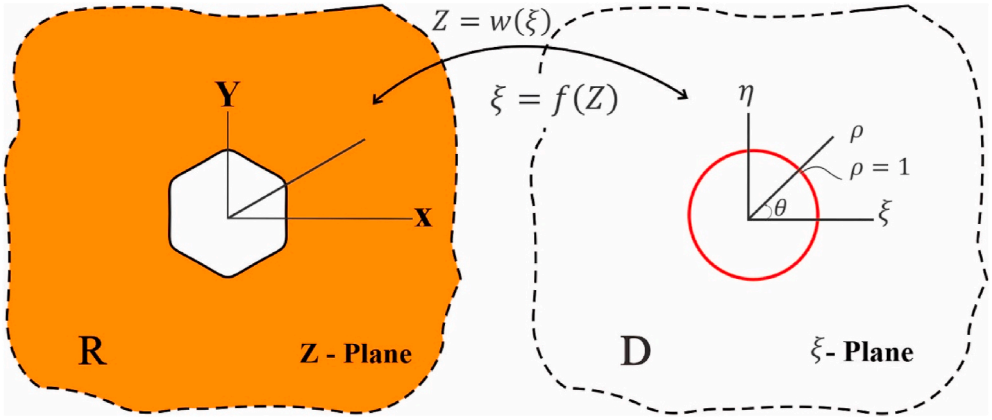

Fig. 3. Conformal mapping.

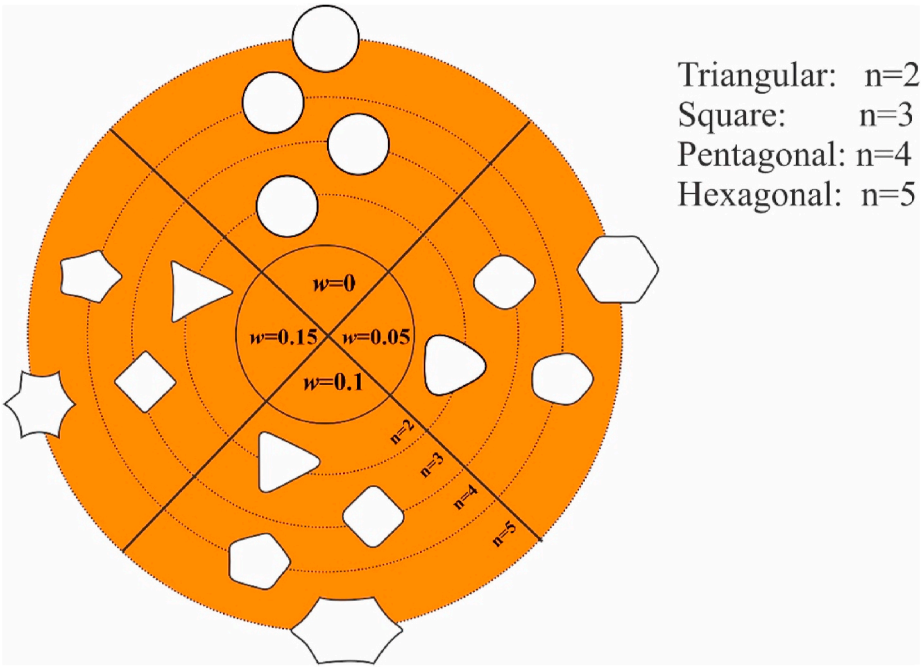

Fig. 4. Cutout shapes with various values of the parameters n and w.

$$z_k = w(\xi) = x + \mu_k y \quad (k = 1, 2, t) \tag{58}$$

in which x and y represent the Cartesian coordinates in the laminate with non-circular cutout and can be represented in terms of θ using Eq. (59) (Jafari et al., 2016).

$$\begin{aligned} x &= \lambda(\cos\theta + w\cos(n\theta)) \\ y &= \lambda(c\sin\theta - w\sin(n\theta)) \end{aligned} \tag{59}$$

In Eq. (58), μ_k are the roots of the characteristic equation as defined in Eq. (20) and ξ is defined in Eq. (60).

$$\xi = \rho e^{i\theta} = \rho(\cos\theta + i\sin\theta) \tag{60}$$

For a unit circle $\rho = 1$. In Eq. (59), λ controls only the size of the cutout and the value of this parameter has no effect on the stress distribution around the cutout within an infinite plate, hence it was considered as unity ($\lambda = 1$). Moreover, the parameters c and w determine the aspect ratio and the corner curvature (bluntness) of the cutout, respectively. Fig. 4 shows how the parameters n and w can affect the cutout shape. Considering the cutout corner curvature in the range of $0 \leq w < 1/n$ ensures that there is no loop in the cutout shape in which n determines the cutout geometry as defined in Fig. 4.

The conformal mapping function for a non-circular cutout is determined as Eq. (61) using Euler's equation and Eq. (59).

$$z_k = w(\xi) = \frac{\lambda}{2}\left(\Delta_{1k}\xi + \Delta_{2k}\xi^{-1} + \Delta_{3k}\xi^{n} + \Delta_{4k}\xi^{-n}\right) \tag{61}$$

in which $\Delta_{ik,(i=1,2,3,4)}$ are as below:

$$\begin{aligned} \Delta_{1k} &= \frac{\lambda}{2}[(1 - ic\mu_k)\cos\beta - (ic + \mu_k)\sin\beta] \\ \Delta_{2k} &= \frac{\lambda}{2}[(1 + ic\mu_k)\cos\beta + (ic - \mu_k)\sin\beta] \\ \Delta_{3k} &= \frac{\lambda w}{2}[(1 + i\mu_k)\cos\beta + (i - \mu_k)\sin\beta] \\ \Delta_{4k} &= \frac{\lambda w}{2}[(1 - i\mu_k)\cos\beta - (i + \mu_k)\sin\beta] \end{aligned} \tag{62}$$

Finally, to model the cutout rotation, the parameter (β) is introduced into formulations by Eq. (63).

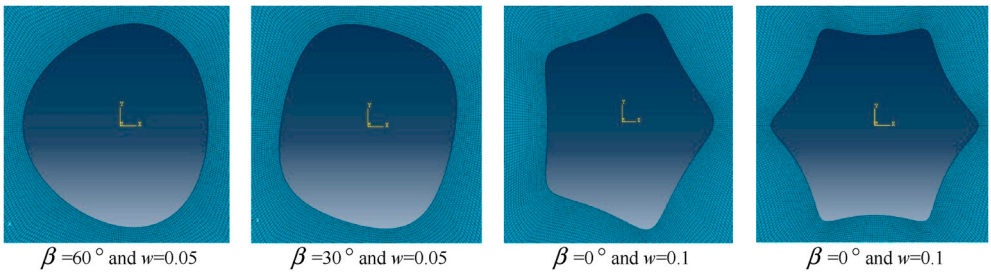

Fig. 5. Mesh refinement for the laminates with non-circular cutout.

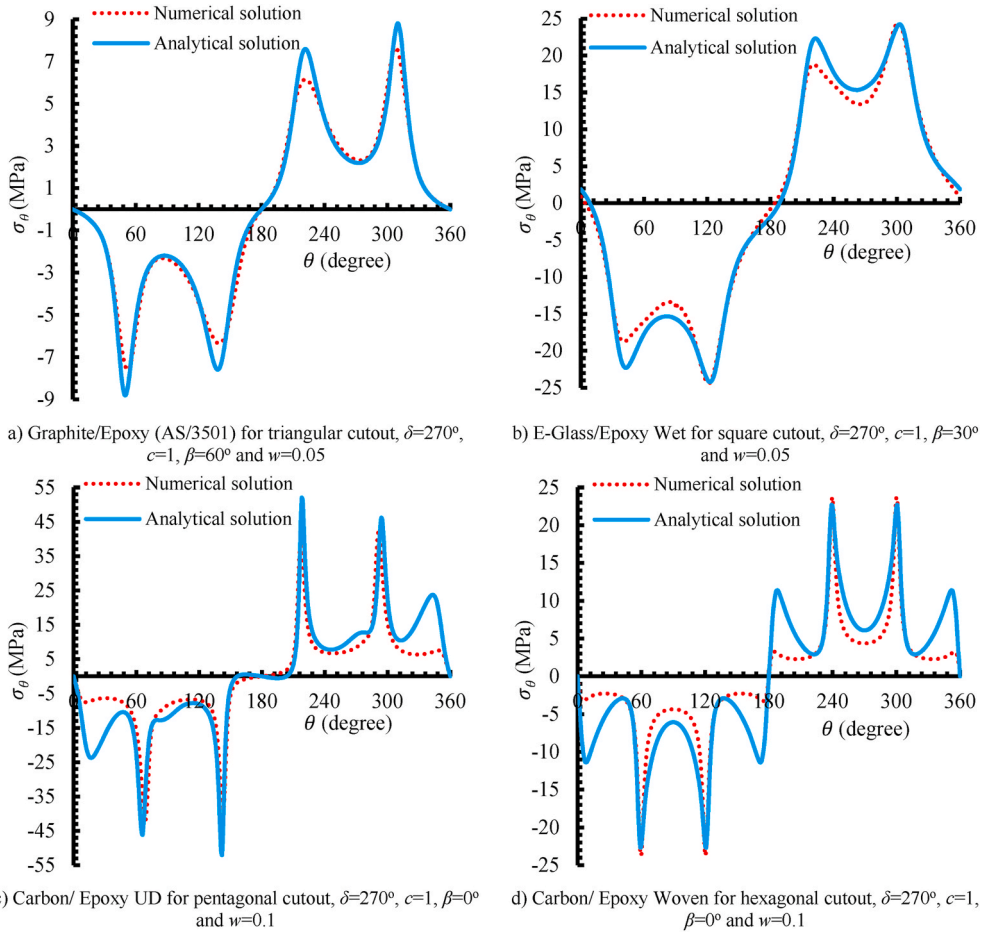

Fig. 6. Comparison between the finite element and analytical results for different materials and cutouts.

$$\begin{Bmatrix} X \\ Y \end{Bmatrix} = \begin{bmatrix} \cos\beta & \sin\beta \\ -\sin\beta & \cos\beta \end{bmatrix} \begin{Bmatrix} x \\ y \end{Bmatrix} \tag{63}$$

in which β is the cutout angular position (i.e. the cutout orientation) and x and y are the Cartesian coordinates. It should be noted that β determines the cutout orientation while θ is the angular position around the cutout.

4. Validation of the analytical solution

To validate the analytical solution obtained in this study, finite element numerical analyses were conducted using ABAQUS finite element code. Three-dimensional finite element models for the perforated composite laminates were developed. The four-noded quadrilateral elements (S4R) were used. To obtain the exact geometric shape of cutout, MATLAB software was employed. The edges of cutouts were considered thermally insulated. Moreover, a uniform heat flux with a magnitude of 200 W/m^2 was applied on the top side of the plate and a uniform heat flux with a magnitude of −200 W/m^2 was applied on the opposite side of the plate.

Fig. 5 shows the mesh refinement for several perforated laminates. A mesh sensitivity study was undertaken to obtain an acceptable mesh size. Fig. 6 compares the analytical and numerical results.

The results illustrated in Fig. 6 are for the laminates with a stacking sequence of $[45/\text{-}45]_s$ and made of different materials of Graphite/Epoxy (AS/3501), E-Glass/Epoxy Wet, Carbon/Epoxy UD and Carbon/Epoxy Woven containing a cutout with different geometries of triangular, square, pentagonal and hexagonal. In Fig. 6, the analytical and numerical tangential stress distributions versus the angular position (θ) on the border of cutouts are plotted. According to Fig. 6, a reasonable agreement was found between the analytical and numerical results validating the proposed analytical solution.

Table 1
Material properties of the composite laminates (Jafari and Jafari, 2019).

Material	E_{11} (GPa)	E_{22} (GPa)	G_{12} (GPa)	υ_{12}	α_{11} (K^{-1})	α_{22} (K^{-1})	K_{11} ($Wm^{-1}K^{-1}$)	K_{22} ($Wm^{-1}K^{-1}$)
Graphite/Epoxy (AS/3501)	144.8	9.7	4.1	0.3	-3×10^{-6}	2.8×10^{-5}	4.62	0.72
E-Glass/Epoxy Wet	35	9	4.7	0.28	5.5×10^{-6}	2.5×10^{-5}	2.2	1.1
Carbon/Epoxy Woven	91.82	91.82	19.5	0.05	2.5×10^{-6}	2.5×10^{-6}	3.5	2.6
Carbon/Epoxy UD	200	9.45	5.5	0.27	0.4×10^{-6}	30×10^{-6}	0.7	1.21
$E_{33} = E_{22},\ G_{12} = G_{13} = G_{23},\ \nu_{12} = \nu_{13} = \nu_{23},\ \alpha_{33} = \alpha_{22},\ K_{33} = K_{22},\ K_{12} = 0$								

5. Results and discussion

In the design of perforated composite laminates under thermal loading, predicting the thermal stress distribution induced around a non-circular cutout is important. In this study, the effects of the geometrical parameters on the thermal stress distribution surrounding the triangular, square, pentagonal and hexagonal cutouts in a symmetric composite laminate under uniform heat flux were analytically studied. To study the effects of different parameters on the thermal stress distribution in a perforated multilayer composite plate, the normalized maximum thermal stress was defined as $\sigma_{norm} = \frac{\sigma_{\theta,\max} \times k_x}{A(1,1) q_0 \lambda |\alpha_x|}$, in which $\sigma_{\theta,max}$ is the maximum tangential stress induced around the cutout, q_0 is the heat flux, $|\alpha_x|$ is the thermal expansion coefficient of the laminate in x direction, k_x is the heat conduction coefficient of the laminate in x direction, $A(1,1)$ is the first entry of the in-plane stiffness matrix. In each perforated multilayer composite plate with a specific cutout, the highest and the lowest thermal stress values ware called undesirable and desirable stresses, respectively. The mechanical properties of the used materials are presented in Table 1.

A quasi-triangular cutout was considered under uniform heat flux. The effects of different parameters of the cutout bluntness (w), the cutout rotation angle (β), the cutout aspect ratio (c) and the composite material were studied on the thermal stress distribution in a multilayer composite plate with a stacking sequence of $[45/-45]_s$ containing a polygonal cutout with different number of sides using the analytical method. To study the effect of different parameters on the thermal stress distribution around the cutout, only one parameter was varied and the values of the other parameters were considered fixed. The default values of the parameters were $\delta = 270°$, $w = 0.05$, $\beta = 0°$ and $c = 1$.

5.1. The cutout aspect ratio

The effect of the aspect ratio of cutout (c) on the normalized

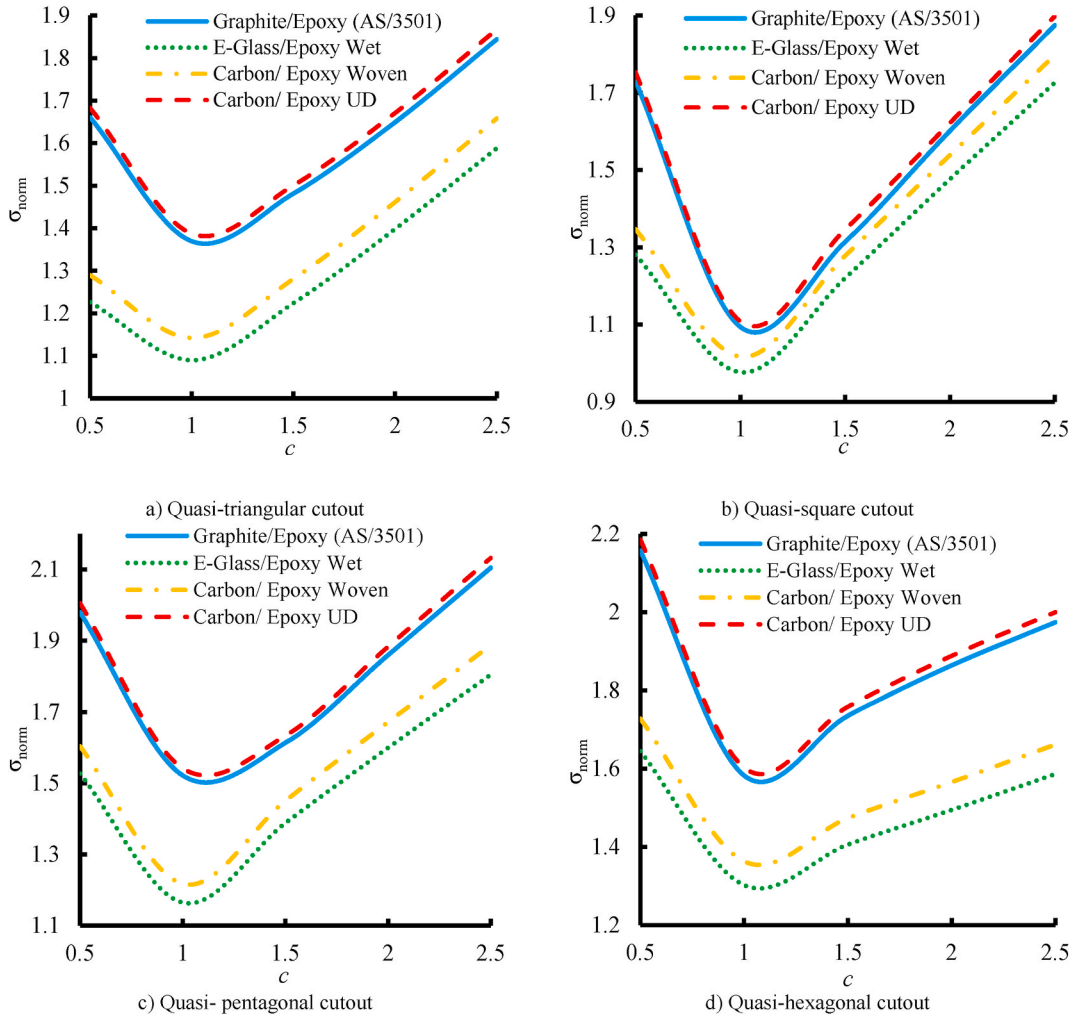

Fig. 7. Comparison between the normalized maximum thermal stress versus cutout aspect ratio curves for the perforated composite laminates with different cutouts.

Table 2
Normalized maximum thermal stress values around the cutout with different aspect ratios.

c	E-Glass/Epoxy Wet				Carbon/Epoxy UD			
	Quasi-triangular	Quasi-square	Quasi-pentagonal	Quasi-hexagonal	Quasi-triangular	Quasi-square	Quasi-pentagonal	Quasi-hexagonal
	σ_{norm}	σ_{norm}	σ_{norm}	σ_{norm}	σ_{norm}	σ_{norm}	σ_{norm}	σ_{norm}
0.5	1.2262	1.2809	1.5269	1.6448	1.6827	1.7527	2.0051	2.1853
1	1.0896	0.9766	1.1647	1.3022	1.3873	1.1082	1.5417	1.6025
1.5	1.2238	1.2276	1.3881	1.4058	1.5009	1.3463	1.6333	1.7580
2	1.3982	1.4768	1.5993	1.4944	1.6710	1.6223	1.8833	1.8881
2.5	1.5881	1.7263	1.8047	1.5861	1.8676	1.8984	2.1324	1.9998

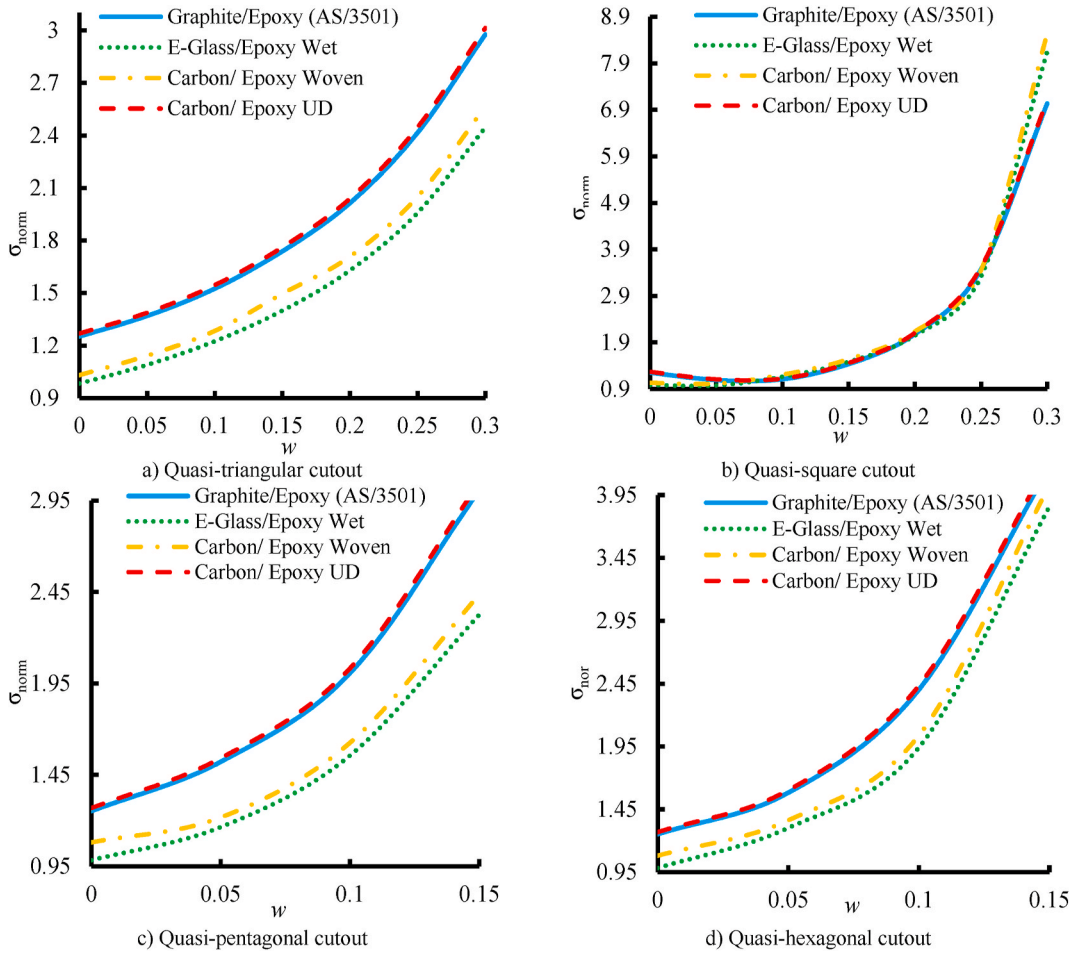

Fig. 8. Comparison between the normalized maximum thermal stress versus cutout bluntness curves for the perforated composite laminates with a) quasi-triangular cutout, b) quasi-square cutout, c) quasi-pentagonal cutout, d) quasi-hexagonal cutout.

maximum thermal stress around a polygonal cutout in a perforated laminated composite is illustrated in Fig. 7. To study the effect of the cutout aspect ratio, the cutout bluntness and rotation angle were considered fixed as $w = 0.05$ and $\beta = 0°$, respectively. As can be seen in Fig. 7, for all materials, by increasing the cutout aspect ratio value up to 1, the maximum thermal stress decreased while further increasing the parameter c resulted in higher maximum thermal stresses. Thus, the minimum thermal stress concentration was achieved at $c = 1$ for different materials. As can be seen in Fig. 7, amongst the materials considered in this study, the laminate made of E-glass/epoxy Wet experienced the minimum thermal stress concentration while the laminate made of Carbon/epoxy UD had the maximum thermal stress concentration, irrespective of the cutout shape and geometry.

Table 2 lists the values of the normalized maximum thermal stress for different cutout aspect ratios and for the E-glass/epoxy Wet and Carbon/Epoxy UD materials. As can be seen in Table 2, amongst different cutout shapes studied, the quasi-square cutout resulted in the minimum thermal stress concentration while the quasi-hexagonal cutout let to the maximum thermal stress concentration.

5.2. The cutout bluntness

The cutout bluntness is a parameter that controls the curvature radius of the polygonal cutout vertices. Fig. 8 compares the normalized maximum thermal stress versus the cutout bluntness curves for the perforated composite laminates made of different materials and with polygonal cutouts with different number of sides. To study the effect of the cutout bluntness, the cutout aspect ratio and rotation angle were considered $c = 1$ and $\beta = 0°$, respectively. To ensure that there is no loop in the cutout shape, the cutout bluntness parameter should be in the

Table 3
Normalized maximum thermal stress values around the cutout with different bluntness values.

w	E-Glass/Epoxy Wet				Carbon/Epoxy UD			
	Quasi-triangular	Quasi-square	Quasi-pentagonal	Quasi-hexagonal	Quasi-triangular	Quasi-square	Quasi-pentagonal	Quasi-hexagonal
	σ_{norm}	σ_{norm}	σ_{norm}	σ_{norm}	σ_{norm}	σ_{norm}	σ_{norm}	σ_{norm}
0	0.9831	0.9831	0.9831	0.9831	1.2685	1.2685	1.2685	1.2685
0.05	1.0896	0.9766	1.1647	1.3022	1.3873	1.1082	1.5417	1.6025
0.1	1.2243	1.1632	1.556	1.9426	1.5449	1.1238	2.0332	2.4345
0.15	1.3990	1.4832	2.3265	3.8599	1.7615	1.4577	3.0482	4.2258
0.2	1.6292	2.0505	–	–	2.0394	2.1054	–	–
0.25	1.9579	3.3161	–	–	2.4467	3.5132	–	–
0.3	2.4457	8.1503	–	–	3.0128	7.0931	–	–

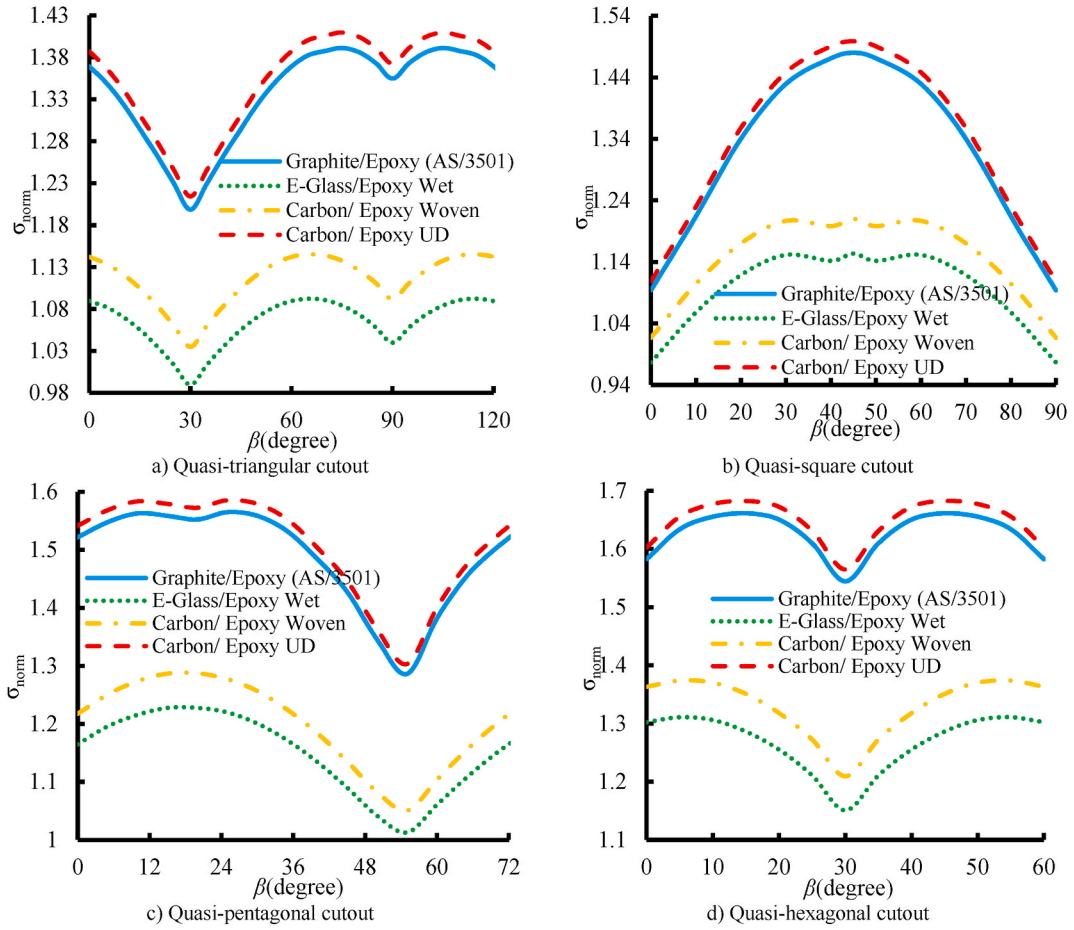

Fig. 9. Comparison between the normalized maximum thermal stress versus cutout rotation angle curves for the perforated composite laminates with different cutouts.

Table 4
Normalized maximum thermal stress values around the cutout with different rotation angles.

β	E-Glass/Epoxy Wet				Carbon/Epoxy UD			
	Quasi-triangular	Quasi-square	Quasi-pentagonal	Quasi-hexagonal	Quasi-triangular	Quasi-square	Quasi-pentagonal	Quasi-hexagonal
	σ_{norm}	σ_{norm}	σ_{norm}	σ_{norm}	σ_{norm}	σ_{norm}	σ_{norm}	σ_{norm}
0	1.0896	0.9766	1.1647	1.3022	1.3873	1.1082	1.5417	1.6025
30	0.9897	1.1514	1.2006	1.1506	1.2143	1.4482	1.5792	1.5647
45	1.0553	1.1536	1.09	1.2861	1.3113	1.4926	1.4466	1.6723
60	1.0896	1.1514	1.0608	1.3022	1.3873	1.4482	1.4004	1.6025
90	1.0399	0.9766	1.2289	1.1506	1.3726	1.1082	1.566	1.5647

range of $0 \leq w < 1/(n\text{-}1)$ for an n-sided polygonal cutout.

As can be seen in Fig. 8, the normalized maximum stress value was increased by increasing the cutout bluntness and the minimum thermal stress concentration was obtained for the circular cutouts (i.e. $w = 0$) in the laminates with quasi-triangular, quasi-pentagonal and quasi-hexagonal. However, for the laminate with a quasi-square cutout, the minimum thermal stress concentration was obtained for the laminates with a cutout having the bluntness of 0.05 and not for the circular cutout. Moreover, the dependency of the normalized maximum thermal stress value on the cutout bluntness for the laminate with a quasi-square cutout was found to be lower compared to the other cutout shapes within the range of $0 \leq w \leq 0.25$. Table 3 presents the values of the normalized maximum thermal stress for different cutouts and different bluntness values for the E-glass/epoxy Wet and Carbon/Epoxy UD materials.

5.3. The cutout rotation angle

The cutout rotation angle (β) determines the angular position of the cutout with respect to the horizontal axes and can affect the thermal stress distribution around the cutout. The effect of the rotation angle of cutout (c) on the normalized maximum thermal stress around a polygonal cutout in a perforated laminated composite is illustrated in Fig. 9.

To study the effect of the cutout rotation angle, the cutout bluntness and aspect ratio were considered $w = 0.05$ and $c = 0$, respectively. It should be noted that for any regular polygon, there is a rotational symmetry angle by which if the polygon is rotated, the original shape will be obtained.

The rotational symmetry angle for an n-sided regular polygon is 360/n. Therefore, the rotational symmetry angles of triangular, square, pentagonal and hexagonal polygons are 120°, 90°, 72° and 60°, respectively, thus the range of the cutout rotation angle for each polygonal cutout in Fig. 9 was considered based on the corresponding rotational symmetry angle. As can be seen in Fig. 8, the desirable rotation angle of cutout for the minimum thermal stress concentration was found to be dependent on the cutout shape.

Table 4 presents the values of the normalized maximum thermal stress for different cutout rotation angles and for the E-glass/epoxy Wet and Carbon/Epoxy UD materials. As can be seen in Table 4, the desirable rotation angle of the quasi-triangular and quasi-hexagonal cutouts for obtaining the minimum thermal stress concentration was obtained 30°. However, the desirable rotation angle of the quasi-square cutout was 0°, while it was 55° for the quasi-pentagonal cutout, as seen in Fig. 9.

Fig. 10 illustrates the effects of different parameters on the thermal stress distribution around a polygonal cutout within a multilayer composite plate.

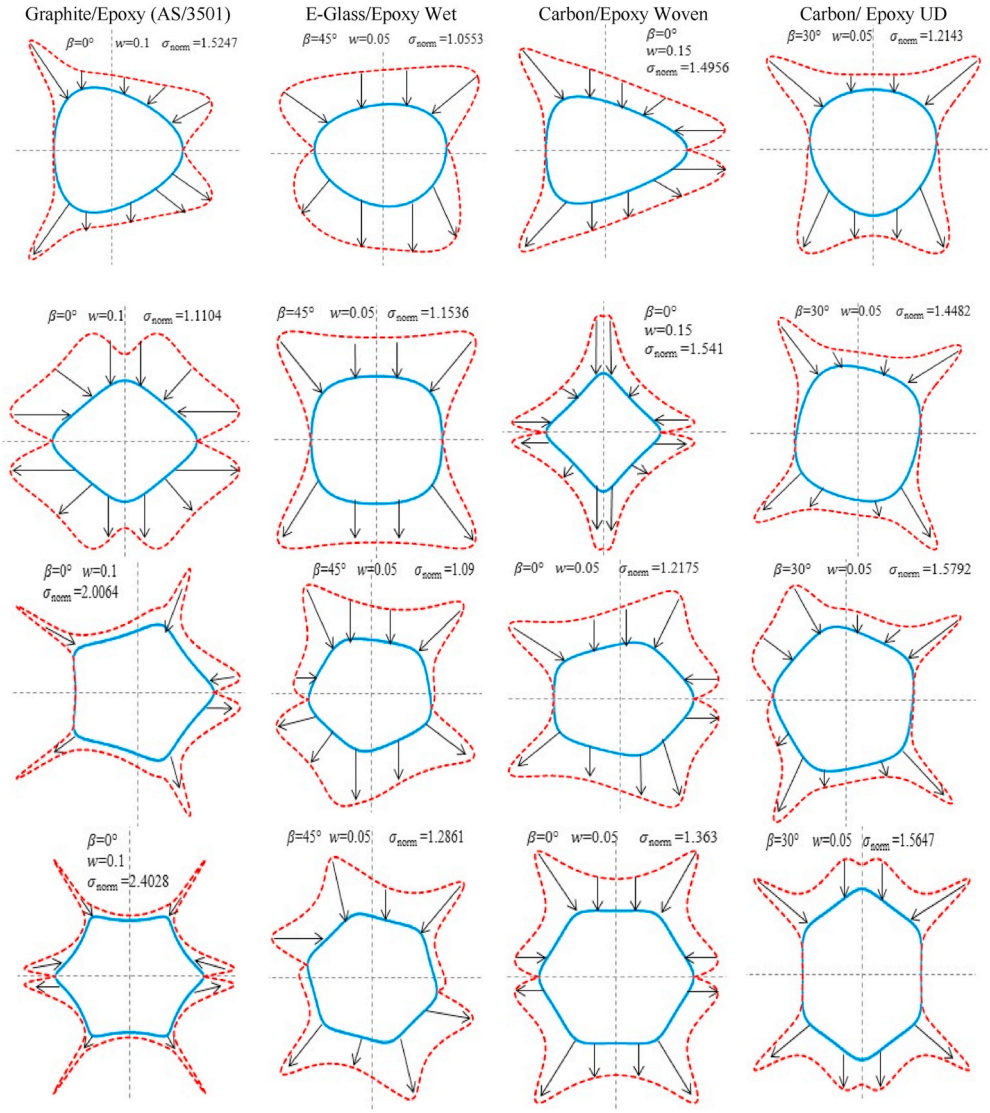

Fig. 10. Thermal stress distributions in a perforated multi-layer composite around the cutout for different parameters.

6. Conclusions

The thermal stress distribution around a polygonal cutout within a multilayer composite plate was studied using an analytical method based on the Lekhnitskii complex variable method and conformal mapping technique. It was assumed that the composite laminate was subjected to uniform heat flux and the cutout edges were thermally insulated. The analytical method was validated against the finite element results. The results showed that increasing the cutout aspect ratio up to 1 decreased the thermal stress concentration and further increasing it resulted in higher thermal stresses. However, the effect of the angular position of cutout was found to be considerably depended on the cutout shape. The quasi-triangular, quasi-square, quasi-pentagonal and quasi-hexagonal cutouts with the angular positions of 30°, 0°, 60° and 30° imposed the minimum thermal stress concentrations on the composite laminate. Investigating the effect of the cutout corner bluntness revealed that a quasi-square cutout with a bluntness of $w = 0.05$ can provide lower thermal stress concentration for a composite laminate compared to the circular cutout. Amongst the laminate materials studied in this paper, the laminate made of the E-Glass/Epoxy experienced the minimum thermal stress concentration and the laminate made of the Carbon/Epoxy UD had the maximum thermal stress concentration.

Author statement

Mohammad Hossein Bayati Chaleshtari: Conceptualization; Methodology; Data curation; Formal analysis; Validation; Visualization; Roles/Writing – original draft, **Hadi Khoramishad:** Conceptualization; Methodology; Supervision; Writing – review & editing.

Declaration of competing interest

The authors declare that they have no known competing financial interests or personal relationships that could have appeared to influence the work reported in this paper.

References

Bayati Chaleshtari, M.H., Jafari, M., 2017. Optimization of finite plates with polygonal cutout under in-plane loading by gray wolf optimizer. J. Strain Anal. Eng. Des. 52, 365–379. https://doi.org/10.1177/0309324717716270.

Bhullar, S.K., Wegner, J.L., 2009. Thermal stresses in a plate with hyperelliptical hole. J. Eng. Technol. Res. 1, 152–170.

Cai, H., Lu, A., zhong, Ma, cai, Y., 2019. Shape optimization of two interacting holes with different areas in an infinite plate. Eur. J. Mech. Solid. 78, 103844. https://doi.org/10.1016/j.euromechsol.2019.103844.

Chao, C.K., Shen, M.H., 1998. Thermal stresses in a generally anisotropic body with an elliptic inclusion subject to uniform heat flow. J. Appl. Mech. 65, 51. https://doi.org/10.1115/1.2789045.

Hasebe, N., Wang, X., 2005. Complex variable method for thermal stress problem. J. Therm. Stresses 28, 595–648. https://doi.org/10.1080/01495730590932706.

Herakovich, C.T., 1998. Mechanics of Fibrous Composites. Johan Wiley & Sons, University of Virginia, Virginia.

Jafari, M., Bayati Chaleshtari, M.H., 2017. Using dragonfly algorithm for optimization of orthotropic infinite plates with a quasi-triangular cut-out. Eur. J. Mech. Solid. 66, 1–14. https://doi.org/10.1016/j.euromechsol.2017.06.003.

Jafari, M., Jafari, M., 2019. Thermal stress analysis of orthotropic plate containing a rectangular hole using complex variable method. Eur. J. Mech. Solid. 73, 212–223. https://doi.org/10.1016/j.euromechsol.2018.08.001.

Jafari, M., Moussavian, H., Bayati Chaleshtari, M.H., 2018. Optimum design of perforated orthotropic and laminatedcomposite plates under in-plane loading by genetic algorithm. Struct. Multidiscip. Optim. 57, 341–357. https://doi.org/10.1007/s00158-017-1758-5.

Jafari, M., Nazari, M.B., Taherinasab, A., 2016. Thermal stress analysis in metallic plates with a non-circular hole subjected to uniform heat flux. Eur. J. Mech. Solid. 59, 356–363. https://doi.org/10.1016/j.euromechsol.2016.05.004.

Joshi, P.V., Gupta, A., Jain, N.K., Salhotra, R., Rawani, A.M., Ramtekkar, G.D., 2017. Effect of thermal environment on free vibration and buckling of partially cracked isotropic and FGM micro plates based on a non classical Kirchhoff's plate theory: an analytical approach. Int. J. Mech. Sci. 131–132, 155–170. https://doi.org/10.1016/j.ijmecsci.2017.06.044.

Lal, A., Singh, H.N., Shegokar, N.L., 2012. FEM model for stochastic mechanical and thermal postbuckling response of functionally graded material plates applied to panels with circular and square holes having material randomness. Int. J. Mech. Sci. 62, 18–33. https://doi.org/10.1016/j.ijmecsci.2012.05.010.

Lekhnitskii, S.G., 1969. Anisotropic Plates. Gordon and Breach Science, New York https://doi.org/0677206704.

Moure, M.M., García-Castillo, S.K., Sánchez-Sáez, S., Barbero, E., Barbero, E.J., 2017. Matrix cracking evolution in open-hole laminates subjected to thermo-mechanical loads. Compos. Struct. 183, 510–520. https://doi.org/10.1016/j.compstruct.2017.05.059.

Mousanezhad Viyand, D., Yazdani Sarvestani, H., Nosier, A., 2013. Stress analysis in symmetric composite laminates subjected to shearing loads. Int. J. Mech. Sci. 75, 16–25. https://doi.org/10.1016/j.ijmecsci.2013.06.010.

Muskhelishvili, N., 1954. Some Basic Problems of the Mathematical Theory of Elasticity. Springer Netherlands, Dordrecht.

Nageswara Rao, D.K., Ramesh Babu, M., Raja Narender Reddy, K., Sunil, D., 2010. Stress around square and rectangular cutouts in symmetric laminates. Compos. Struct. 92, 2845–2859. https://doi.org/10.1016/j.compstruct.2010.04.010.

Natsuki, T., Natsuki, J., 2019. Analysis of thermal stress in graphene nanoribbons coated with nano-film. Eur. J. Mech. Solid. 75, 21–26. https://doi.org/10.1016/j.euromechsol.2018.11.002.

Ozisik, N.M., 1993. Heat Conduction, second ed. John Wiley & Sons, New York, NY.

Rasouli, M., Jafari, M., 2016. Thermal stress analysis of infinite anisotropic plate with elliptical hole under uniform heat flux. J. Therm. Stresses 39, 1341–1355. https://doi.org/10.1080/01495739.2016.1216038.

Savin, G.N., 1961. Stress Distribution Around Holes. Pregamon Press, New York.

Sayman, O., 2005. Elastic-plastic stress analysis of symmetric aluminum metal-matrix composite laminated plates under thermal loads varying linearly. Compos. B Eng. 36, 61–72. https://doi.org/10.1016/j.compositesb.2004.02.002.

Sharma, D.S., 2015. Stresses around polygonal hole in an in finite laminated composite plate. Eur. J. Mech./A Solids 54, 44–52. https://doi.org/10.1016/j.euromechsol.2015.06.004.

Tarn, J.Q., Wang, Y.M., 1993. Thermal stresses in anisotropic bodies with a hole or a rigid inclusion. J. Therm. Stresses 16, 455–471. https://doi.org/10.1080/01495739308946240.

Ukadgaonker, V.G., Rao, D.K.N., 2000. A general solution for stresses around holes in symmetric laminates under inplane loading. Compos. Struct. 49, 339–354. https://doi.org/10.1016/S0263-8223(00)00070-2.

Zeng, X. tai, Lu, A. zhong, Zhang, N., 2018. Analytical stress solution for an infinite plate containing two oval holes. Eur. J. Mech. Solid. 67, 291–304. https://doi.org/10.1016/j.euromechsol.2017.09.011.